ACS ES&T Water

Open Access

pubs.acs.org/estwater

Article

Microwave-Assisted Synthesis of Hydrangea-Like Graphitic Carbon Nitride as an Effective Photocatalyst in Dye Degradation and Hydrogen Generation

Kok-Hou Tan, Chen-Yu Lin, and Yang-hsin Shih*

Cite This: *ACS EST Water* 2024, 4, 5902−5912

Read Online

ACCESS | Metrics & More | Article Recommendations | Supporting Information

ABSTRACT: Photocatalysis is a process that has been extensively studied for its great potential in environmental remediation and energy production. In this study, a two-step microwave-assisted synthesis approach was employed to prepare graphitic carbon nitrides (GCNs) as an environmentally friendly metal-free photocatalyst. A porous, high surface area, graphitic carbon nitride (C_2N_3) photocatalyst with unique hydrangea-like morphology (CNUMW) was successfully synthesized with a yield 5 times greater than directly calcined GCN. The enhanced yield was attributed to the formation of polar functional groups containing a biuret and cyanuric acid mixture as the intermediate prior to microwave pretreatment, which effectively reduced the loss of decomposition gases during the thermochemical conversion process. The as-synthesized CNUMW has a smaller band gap, a larger surface area, and a higher light absorption capacity near the Urbach energies, which are responsible for its superior activity in photocatalytic dye degradation (k = 0.216 min^{-1}) compared to non-microwave pretreated counterparts. Scavenging tests revealed that the CNUMW-catalyzed photocatalytic reaction undergoes a superoxide-mediated pathway, which can be increased with the addition of a hole scavenger. The resulting CNUMW can also catalyze hydrogen production at an enhanced rate of 1.93 mmol g^{-1} h^{-1}. The novel urea-derived flower-like C_2N_3 demonstrates great potential in simultaneous wastewater treatment and energy production..

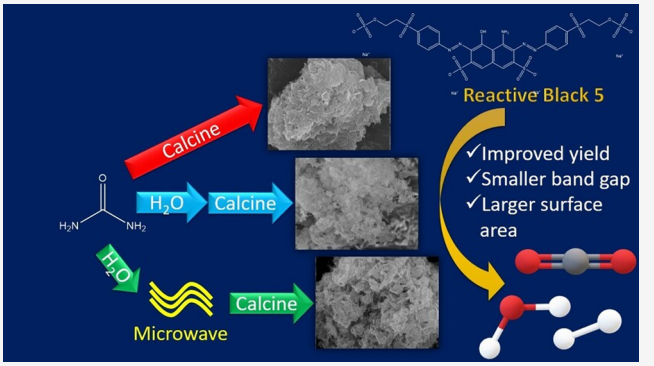

KEYWORDS: *carbon nitrides, microwave-assisted synthesis, water splitting, photocatalysis, dye removal*

1. INTRODUCTION

Photocatalysts are semiconducting materials that accelerate chemical reactions under electromagnetic radiation. When exposed to light, the valence electrons of these catalytic materials gain enough energy to be promoted to the conduction band, leaving behind positive holes. These charge carriers are then utilized in catalyzing photochemical reactions, such as degradation of organic pollutants, hydrogen evolution, disinfection, chemical transformations, and detoxification. Numerous metal- and nonmetal-based photocatalysts have been developed and evaluated for specific applications. Carbon-based photocatalysts, for instance, graphene oxide, carbon aerogel, metal-doped biochar, modified activated carbon, carbon dots, and carbon nitride, have drawn the scientific community's attention due to their biocompatibility and nontoxic nature.[1] Carbon nitride has been one of the most studied materials owing to its visible-light absorption, simple synthesis, stability, and ease of structural modifications.

Carbon nitrides were reported by Berzelius and were named melon by Liebig in 1834.[2] Several polymorphs of carbon nitrides have been synthesized, including g-C_3N_4, C_2N, C_3N, and C_5N_2.[3] These two-dimensional semiconducting materials have been widely studied in photocatalytic water decontamination processes. For instance, g-C_3N_4 with a narrow band gap (2.7 eV) has been fabricated into membranes to treat wastewater.[4] Different nanostructured g-C_3N_4, such as ultrathin nanosheets, nanorods, porous spheres, nanotubes, and quantum dots were prepared for photocatalytic reduction of toxic metal ions, H_2 production, and degradation of organic pollutants.[5] Various strategies have been adopted to further increase the photocatalytic activity of carbon nitrides. Metal doping, nonmetal doping, hybridizing with carbon materials, and coupling with other semiconductors were among the strategies used to enhance the photocatalytic performance of graphitic carbon nitrides.[6]

Received: September 12, 2024
Revised: November 17, 2024
Accepted: November 18, 2024
Published: November 26, 2024

Literature suggests that the precursor plays a vital role in determining the physicochemical and photocatalytic properties of carbon nitrides. Song et al. successfully produced a large surface area of g-C_3N_4 (114 m^2 g^{-1}) by a one-step polycondensation process that utilizes urea as the precursor. The resulting carbon nitride was able to completely degrade 10 mg L^{-1} of rhodamine B within 20 min of UV−visible light irradiation.[7] Fidan and coworkers studied the influence of precursors on the properties of g-C_3N_4.[8] The highest synthesis yield was obtained when dicyandiamide was used (∼45%), while urea and thiosemicarbazide produce much lower amounts of graphitic carbon nitrides (4−5.5%). However, the same study showed that urea-derived g-C_3N_4 has a significantly larger specific surface area (139 m^2 g^{-1}) than dicyandiamide (22.24 m^2 g^{-1}) and thiosemicarbazide-derived (18.63 m^2 g^{-1}) counterparts. Wang et al. demonstrated that urea and tetracyanoethylene copolymerized g-C_3N_4 performed better than bulk g-C_3N_4 by achieving a rate constant of 0.0317 min^{-1} for Orange II degradation under visible light.[9] Another experiment by Liu et al. prepared g-C_3N_4 with melamine, a melamine-urea mixture, and melamine-cyanuric acid.[10] It was depicted that melamine-urea-derived g-C_3N_4 with a significantly larger BET surface area (98.04 m^2/g) than the two other candidates (11−12 m^2/g) outperformed them with a norfloxacin photodegradation rate constant of 1.50 min^{-1}. These examples showed that carbon nitrides derived from urea and its mixture have a higher photocatalytic activity and are viable for photocatalysis applications.

Although urea-based carbon nitrides possess higher photocatalytic activity, they suffer from a low production yield, as low as 1%, because of the gasification of urea and carbon nitride during the pyrolysis process.[11] Shi and coworkers increase the yield of urea-derived polymeric graphitic carbon nitride by 3 times via co-condensation with tetraethylorthosilicate (TEOS).[12] While a study by Ye et al. showed that mixing urea and dicyandiamide can also enhance the surface area and yield of carbon nitride by 4.9 and 3.4 times, respectively.[13] The resulting carbon nitride photocatalyst had a hydrogen production activity that was 3.36 times higher than that of the bulk carbon nitride. However, while the second precursor helps to improve the yield, it can reduce the surface area at the same time.[14]

In this study, we attempt to improve the yield and photocatalytic activity of urea-derived carbon nitride through the microwave pretreatment of a damp urea precursor before calcination. The resulting carbon nitride was characterized and evaluated for its photocatalytic activity in both dye removal and hydrogen production reactions to exploit its water treatment and energy generation potential.

2. EXPERIMENTAL SECTION

2.1. Materials. Reagent grade urea (Bioshop, ≥99.0%) was purchased from Bioman Scientific Co., Ltd. HPLC grade methanol (Honeywell Burdick & Jackson, ACS/USP reagent, >99.9%) and *tert*-butyl alcohol (*t*-BuOH, J.T.Baker, ACS reagent) were supplied by Dinhaw Enterprise Co., Ltd. and Avantor Performance Materials, Inc., respectively. Ultrapure water (resistivity = 18.2 MΩ·cm) was generated from a Lotun RDI-20 ultrapure water system. Anhydrous sodium sulfate (Na_2SO_4, extra pure, 99.0%), *p*-benzoquinone ($C_6H_4(O)_2$, BQ, 99%), and sodium persulfate ($Na_2S_2O_8$, 98%) of Acros Organic were used in this study. 85% phosphoric acid (H_3PO_4) was received from Merck while ethylenediaminetetraacetic acid disodium salt (EDTA-Na_2, Crown Guaranteed Reagent) was supplied by Yakuri Pure Chemicals Co., Ltd. Reactive black five (RB5) was purchased from Sigma-Aldrich. Hydrochloric acid (HCl, 37%, Reagent grade, ACS reagent) and sodium hydroxide (NaOH, ≥96.0%) used in pH adjustment were obtained from Scharlau and Nacalai Tesque, respectively. The screen-printed electrode (TE100, carbon working electrode, radius = 3 mm, area = 7.1 mm^2) used in the electrochemical measurement was obtained from Zensor R&D Co., Ltd.

2.2. Synthesis of Carbon Nitride. The preparation of directly calcined carbon nitride was as follows. 5 g of urea was weighed in a crucible, covered with a lid, and wrapped with aluminum foil before being subjected to calcination at a ramp rate of 5 °C/min to 550 °C and maintained for 4 h. The resulting carbon nitride powder was ground and denoted as CNU. A similar procedure was adapted to synthesize the water-added counterpart but with an additional step of adding 1 mL of ultrapure water to the urea precursor before the calcination. The calcination product was labeled CNUH2O.

Microwave-assisted carbon nitride synthesis was carried out following a two-step modified protocol of Meng et al.[15] 10 g of urea was transferred to a 75 mL MARSXpress high-throughput vessel, and 1 mL of ultrapure water was added. Microwave treatment was performed in a CEM MARS-5 Microwave Accelerated Reaction System with a ramp time of 15 min to 170 °C at 800 W and held for 15 min. The system was then allowed to cool to room temperature. The resulting mixture was extracted with water and subsequently dried in an oven at 80 °C overnight. The dried product was ground into a powder and denoted as the intermediate. This intermediate was calcined at 550 °C for 4 h at a ramp rate of 5 °C/min. The photocatalyst produced was named CNUMW.

2.3. Characterization. X-ray diffraction (XRD) analysis was performed using a Rigaku Miniflex (Cu K_α = 1.540593 Å, current = 15 mA, voltage = 40 kV) to determine the structure of the as-synthesized catalysts. The texture of catalysts was analyzed using a JEOL JSM-7610F field emission scanning electron microscope (FESEM) equipped with an in-lens Schottky field emission electron gun (15.0 kV) and a Hitachi H7100 transmission electron microscope (75 kV). The nitrogen adsorption−desorption isotherm was measured using a Beckman Coulter SA3100 surface area analyzer, and data were treated in accordance with the Brunauer−Emmett−Teller (BET) analysis. The light absorption ability and band gap energy of photocatalysts were analyzed with diffuse reflectance spectroscopy using a JASCO V670 UV−vis spectrophotometer. Exciton's recombination rate was evaluated via photoluminescence spectroscopy (PL, Hitachi F-7000 FL spectrophotometer, $\lambda_{excitation}$ = 330.0 nm), while elemental composition was measured using an Elementar Unicube organic elemental analyzer. The surface chemical composition of carbon nitride was determined by X-ray photoelectron spectroscopy (Quantes ULVAC-PHIAl, XPS, Al Kα = 1.4 keV) with the C 1s signal calibrated to 284.8 eV. Functional groups of as-synthesized CNUs were compared using a Fourier Transform synchrotron infrared spectrometer (FT-IR, Nicolet 6700, Thermo Fisher Nicolet Instruments, Madison, WI, USA) equipped with a 250 μm × 250 μm liquid nitrogen-cooled mercury−cadmium−telluride (MCT) detector at the TLS 14A1 beamline of the National Synchrotron Radiation Research Centre at Hsinchu, Taiwan. Electrochemical characterization was performed using a CH Instrument 614D electrochemical workstation. A polypropylene-

https://doi.org/10.1021/acsestwater.4c00879
ACS EST Water 2024, 4, 5902−5912

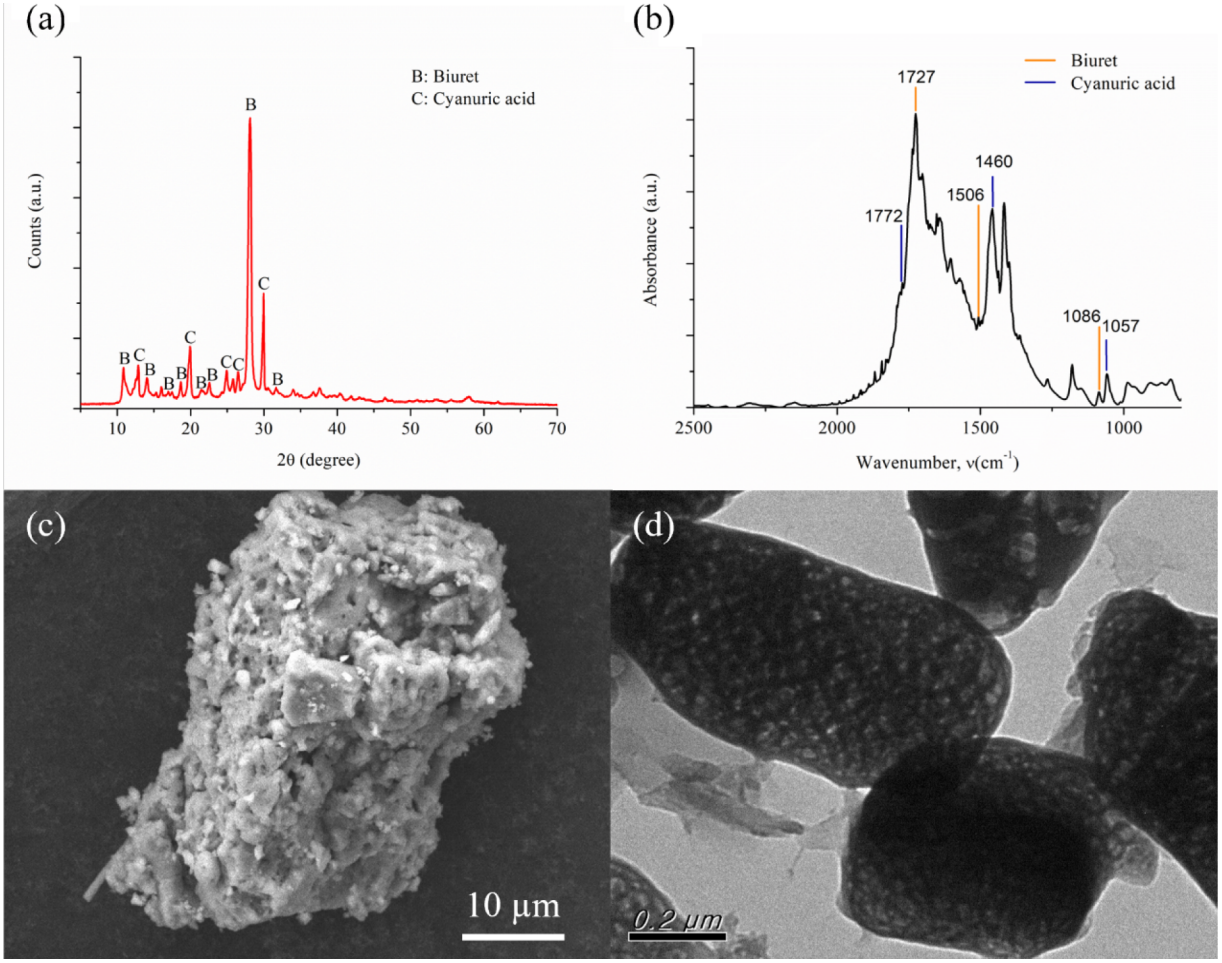

Figure 1. (a) XRD diffractogram, (b) IR spectrum, (c) SEM micrograph, and (d) TEM image of the microwave-treated intermediate.

based screen-printed electrode (TE100) comprising of an Ag reference electrode and a carbon working electrode of 7.1 mm^2 was used together with a 0.1 M Na_2SO_4 electrolyte solution.

2.4. Photocatalysis. The photocatalytic activity of as-synthesized carbon nitride materials in degrading RB5 was evaluated under the irradiation of a 10 W visible light LED lamp equipped with an air-cooling system (Spotlight 60D, λ = 420 nm). A specific amount of photocatalyst was added into 20 mL of an aqueous RB5 solution and allowed to reach adsorption equilibrium in the dark under 30 min of continuous stirring. The reaction mixture was then subjected to photo-irradiation. 2 mL sample aliquot was withdrawn at predetermined time intervals and filtered with a 0.22 μm membrane filter to remove the photocatalyst. The absorbance of the filtrate at λ = 595 nm was measured using a UV−visible spectrophotometer. The effect of catalyst loading, RB5 concentration, and pH was studied to determine the optimum reaction conditions. The pH of the RB5 solution was adjusted to 5.6, 6.1, 7.7, and 9.0 using 0.1 M HCl and 0.1 M NaOH solution. Photocatalytic hydrogen production during RB5 degradation was evaluated using a combination of the water displacement method and GC-TCD analysis. Before the reaction, the precursor mixture was purged with nitrogen gas for 30 min. The gas produced was trapped and analyzed with a GC with a TCD (Agilent 6890N) equipped with a GS-Q column (30 m × 0.530 mm) and helium as a carrier gas. The species that were reactive and responsible for the carbon nitride-catalyzed photodegradation of RB5 were investigated through a scavenging test.

3. RESULTS AND DISCUSSION

3.1. Formation of Carbon Nitride. The formation of hydrangea-like carbon nitride (CNUMW) was investigated by assessing the microwave-treated intermediate. Structural analysis using XRD showed that the urea-derived intermediate was made up of mixed crystalline phases comprising biuret and cyanuric acid (Figure 1a). This is similar to the finding of Gross and Höppe, who performed an *in situ* study on the thermal decomposition of biuret, a major urea pyrolysis intermediate, using temperature-programmed powder XRD and observed a comparable mixed-phase compound when the biuret was heated between 160 and 180 °C.[16]

The IR spectrum of the intermediate also evidenced the existence of both the biuret and the cyanuric acid phases (Figure 1b). Based on the literature, the absorption bands at 1727 and 1772 cm^{-1} were assigned as the C−O stretching band of cyanuric acid and biuret, respectively.[16] In addition, the presence of biuret and cyanuric acid was also proved by the N−H bending bands at 1506 and 1460 cm^{-1}. Intramolecular hydrogen bonding of biuret and cyanuric acid has also helped to differentiate them by showing two distinct rocking vibrations at 1086 and 1057 cm^{-1}.

The texture and morphology of the microwave-treated intermediate were observed by using electron microscopy. The

https://doi.org/10.1021/acsestwater.4c00879
ACS EST Water 2024, 4, 5902−5912

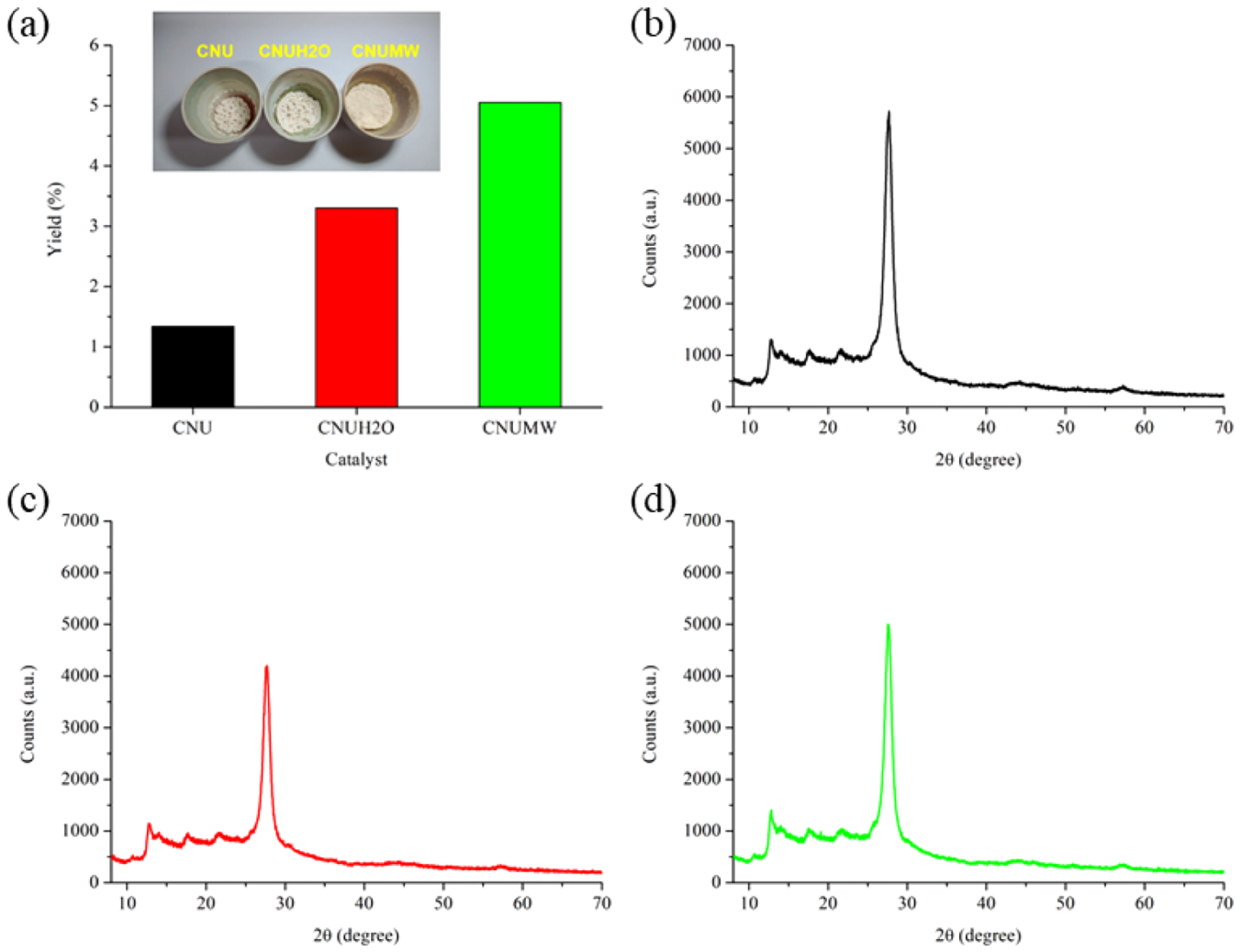

Figure 2. (a). Yield and physical appearance of the as-synthesized carbon nitrides. XRD diffractograms of (b) CNU, (c) CNUH2O, and (d) CNUMW.

SEM micrograph of the intermediate was made up of bulk porous granules with scattered nanosized intergrowths (Figure 1c). The porous structure was confirmed by a TEM image (Figure 1d). The formation of these porous structures was due to the emission of NH_3, H_2O, and CO_2 gas during the thermal treatment of moisturized urea.[17] In addition to pores inherent from the removal of NH_3 and CO_2 gases, the biuret and cyanuric acid phases in the microwave-treated intermediate have different decomposition temperatures of 190−250 °C and 250−360 °C, which allowed them to decompose and condense separately to avoid close stacking.[18] Liu et al. produced a porous g-C_3N_4 from a urea-melamine mixed precursor, which has a BET surface area that is more than eight times larger than that of the g-C_3N_4 prepared from melamine only.[10] Another study by Wang and Yang has also observed a five-times increase in surface area when mixing urea and cyanamide.[19] They explained the improvement in surface area as the result of gas escaping, while the enhanced yield was due to the formation of polar groups that prevent losses from NH_3 and CO_2 escaping. The same rationale can also be applied to this study, where the N−H group in biuret and the O−H group in cyanuric acid are both capable of capturing NH_3 and CO_2 through hydrogen bonding and dipole−dipole interaction (Figure 1b). Hence, it was suggested that a higher number of polar hydrogen bonding species in the precursor can effectively improve the yield of carbon nitride by retaining decomposition product molecules during the calcination process for thermal polymerization−condensation of g-C_2N_3. Characterization results evidenced that the formation of a mixed-phase intermediate is the key to the high porosity and increased yield of CNUMW.

3.2. Carbon Nitride Yield. Urea-derived carbon nitride is known to be superior in photocatalytic activity to those prepared from other precursors.[20] However, it suffers from a much lower yield than those of other preparation techniques. Microwave-assisted two-step synthesis was employed in this study to increase the yield of carbon nitride while retaining its photocatalytic activity. Comparing the production yield of CNU, CNUH2O, and CNUMW, it was demonstrated that the proposed strategy successfully improves the percentage yield (Figure 2a). While it was observed that the addition of water can increase the yield of carbon nitride 3-fold, pretreating urea with microwaves further enhances the yield, with the CNUMW yield five times higher than that of directly calcined CNU. The potential changes of structure and morphology in conjunction with the yield enhancement were evaluated by examining the physicochemical, optical, and electrochemical properties of the CNUs.

https://doi.org/10.1021/acsestwater.4c00879
ACS EST Water 2024, 4, 5902−5912

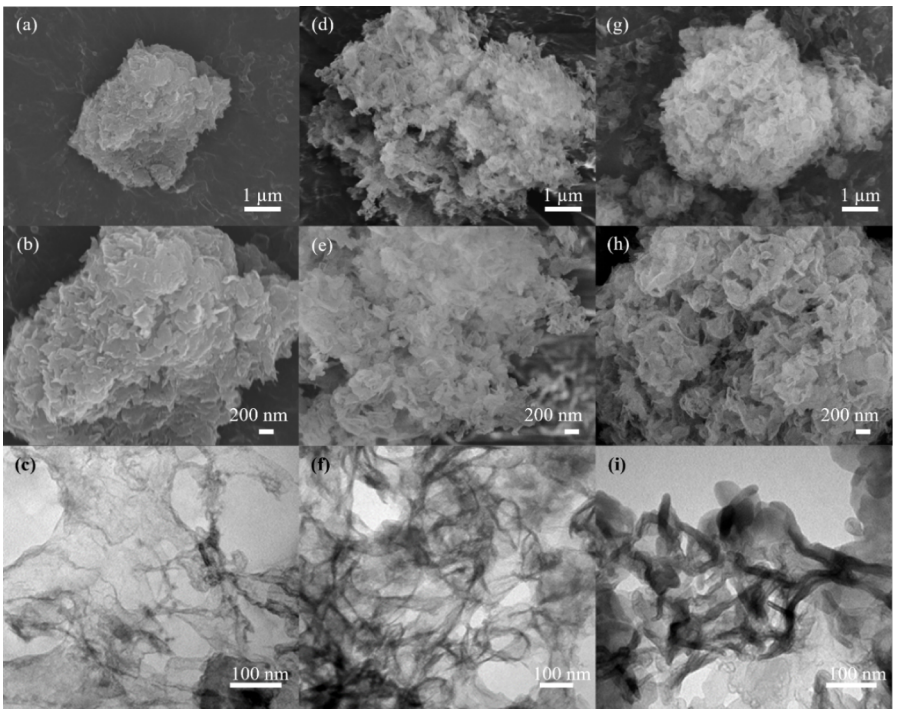

Figure 3. SEM images of CNU (a, b), CNUH2O (d, e), and CNUMW (g, h). TEM micrographs of (c) CNU, (f) CNUH2O, and (i) CNUMW.

A range of characterization techniques was applied to compare the physicochemical, electrochemical, and optical properties of the three CNUs prepared to correlate them to the photocatalytic performance. The XRD diffractogram of CNUMW (Figure 2d) depicts less intense diffraction peaks than CNU (Figure 2b) at 17.5°, 21.6°, and 27.5°, which were attributed to the (011), (110), and interlayer structural aromatic packing at the (002) plane, respectively.[21] This suggested that the proposed synthesis strategy produced a graphitic carbon nitride with fewer layers of stacking. However, CNUMW has a more extensive periodic intraplanar tri-s-triazine motif stacking, as represented by a more intense (100) diffraction peak at 12.9°.[22]

Based on the SEM micrograph, the CNU was found to be made up of layered plate-like agglomerates (Figure 3a,b). Adding water to the urea before calcination leads to the formation of smaller nanoplates with thicker edges and disordered intergrowth (Figure 3d,e). Similar disordered morphology was observed in CNUMW, but with a high amount of hollow space within the agglomerate, giving rise to its hydrangea-like appearance (Figure 3g,h).

Further investigation with TEM revealed that the plate-like CNU particles are comprised of thin, continuous polymeric sheets with wrinkles (Figure 3c).[23] Modification with water thickened the edge of the CNUH2O nanosheet and interrupted the continuity of the polymeric structure, which was supported by its lower degree of crystallinity (Figure 3f). The magnified image of CNUMW differentiated it from the morphology of CNUH2O in which twisted hollow tubes were formed (Figure 3i).

The textures of prepared CNUs were analyzed using Brunauer–Emmett–Teller (BET) analysis of nitrogen adsorption–desorption isotherms and showed that CNUMW (S_{BET} = 120.7 m^2 g^{-1}, d_p = 5.9 nm) has a 13.9% larger specific surface area (S_{BET}) and a pore size (d_p) that is 96.7% of CNU (S_{BET} = 106.0 m^2 g^{-1}, d_p = 6.1 nm) (Table 1). Unlike CNUH2O, which suffered an abrupt decline in S_{BET}, V_{total}, and pore enlargement, a two-step microwave synthesis successfully produced CNUMW with a larger amount of total pore volume as a result of hollow spacing formation within the highly disordered CNUMW nanoparticles. The porosity and textural properties of the more abundant CNUMW were demonstrated to be comparable to those of CNU.

Table 1. Surface Area and Pore Properties of CNUs

Catalyst	Specific surface area, S_{BET} (m^2 g^{-1})	Total pore volume, V_{total} (cm^3 g^{-1})	Pore size, d_p (nm)
CNU	106.0	0.1623	6.1
CNUH2O	41.6	0.0803	7.7
CNUMW	120.7	0.1776	5.9

Elemental analysis was carried out to compare the composition of the differently prepared CNUs, and the results are displayed in Figure 4a. It was observed that the addition of water slightly reduced the C and H concentration of the as-synthesized CNUH2O while increasing its O content by 18%. Meanwhile, microwave-pretreated CNUMW has 24% less of O and a higher amount of C and H compared to CNU. A previous study by Praus et al. suggested that carbon nitride with lower oxygen content has a larger surface area and higher photocatalytic activity owing to its higher degree of exfoliation and lower amount of surface hydroxyl groups.[24]

It was found that the C/N molar ratio of all CNU prepared was 0.68, which suggested that graphitic C_2N_3 (g-C_2N_3, C/N = 0.67) was formed instead of the widely studied stable graphitic C_3N_4 (g-C_3N_4, C/N = 0.75). This is further confirmed by the negative slope in their Mott–Schottky plots, which corresponded to p-type semiconducting materials (Figure S1).[25] g-C_2N_3 is a soft and p-type semiconductor made up of aromatic pentagonal azide and hexagonal triazine.[26,27] This helps to explain the formation of curved structures in all CNUs and the existence of twisted hollow tubes in the CNUMW (Figure 3a-

https://doi.org/10.1021/acsestwater.4c00879
ACS EST Water 2024, 4, 5902–5912

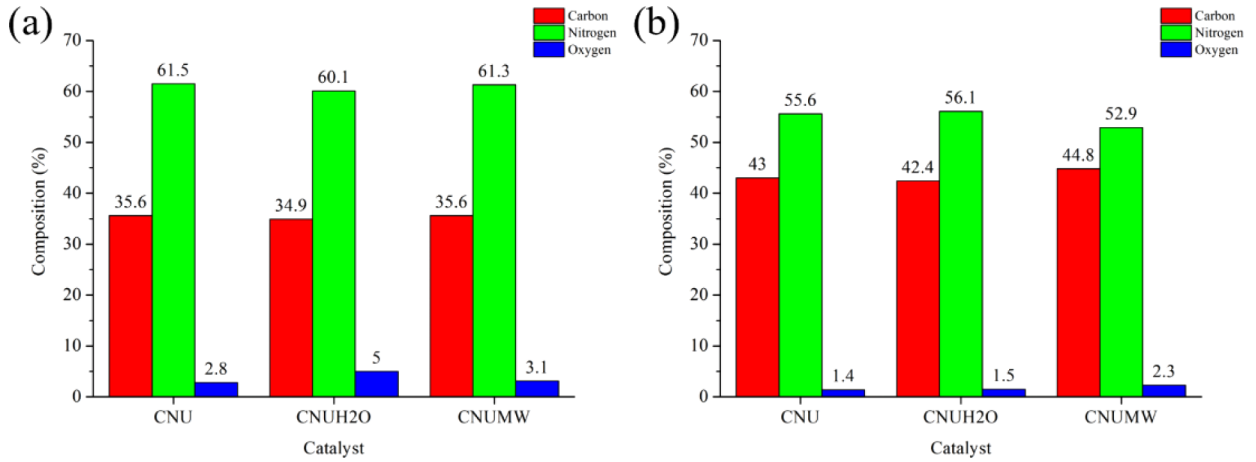

Figure 4. Elemental composition of CNUs in bulk (a) and on the surface (b) measured using an elemental analyzer and XPS, respectively.

i). A similar finding was reported by Tang et al., who prepared curved-leaf-like g-C_2N_3 through a cycloaddition reaction between the nitrile and azide groups of dicyandiamide polymerization products and thermally treated polypyrrole fibers.[27] It was inferred that the presence of azide pentagon is responsible for the discontinuity of the polymeric triazine plane, the exfoliated morphology, and the higher surface area of CNU and CNUMW (Table 1). Nevertheless, urea-derived CNUH2O has a much lower surface area and porosity because it has a higher oxygen content, which indicates a greater number of C−O polar groups that promote the aggregation of carbon nitride particles through dipole−dipole interactions and hydrogen bonding. On the contrary, aggregation of CNU and CNUMW with a lower oxygen content is discouraged by the low interface cohesive energy (−13.67 meV/atom) of the g-C_2N_3 phase.[26]

When the surface elemental composition of CNU was examined using XPS, it was found that the oxygen and nitrogen concentrations are lower, while the carbon content is higher in each photocatalyst (Figure 4b). Nevertheless, it was shown that a large portion of oxygen accounted for particle aggregation and layer stacking in CNU and CNUH2O, but approximately 74% of oxygen in CNUMW was located on the surface. These surface oxygen species are advantageous toward photocatalytic activity as oxygen doping can alter the local electron density and the band gap.[28]

The IR spectra of as-synthesized g-C_2N_3 are depicted in Figure S2. The N−H bond was characterized by three bands at 3000 cm^{-1}, 3300 cm^{-1}, and 889 cm^{-1}.[20,28] The absorption bands at 1533, 1628, and 1682 cm^{-1} were attributed to C═N vibrations.[20,29] The aromatic C−N heterocycles stretching mode was indicated by the peaks at 1225, 1310, 1386, 1430, and 1571 cm^{-1}, while the signal at 813 cm^{-1} belonged to the s-triazine breathing mode.[30,31] Absorption bands located at 1131, 1198, and 1451 cm^{-1} were assigned to the stretching vibrations of C−N and C═N bonds in the polymeric structure.[32] The presence of oxygen-containing C−O groups was evidenced by the peak at 1083 cm^{-1}.[28] IR peaks at 1279 and 1332 cm^{-1} were attributed to nitrogen-containing C−NH_2 stretching and C═NH groups, respectively.[31] Distinct aromatic C−H, aromatic C═C stretching, and CN stretching vibration bands were detected at 875, 1266, and 1497 cm^{-1} in the spectra of CNUMW, respectively.[31,32] The observed functional groups were consistent with the findings of XRD analysis, for which all materials synthesized were graphitic carbon nitrides.

The optical properties of CNUs were analyzed using diffuse reflectance spectroscopy and showed that CNUH2O has a higher light absorption capability than CNU in visible (450−700 nm) and ultraviolet (UV, < 300 nm) regions (Figure 5a). CNUMW has significantly superior UV absorption (200 nm-400 nm), particularly in the UV-A region (315 nm-400 nm). The slope of the band tail (Urbach) energies of the three C_2N_3 indicates there are possible localized similar states that are close to the conduction band, and greater absorption in the UV-A suggests a higher rate of photoexcitation and electron−hole pair formation.[33] The Tauc plots further support this interpretation, as they show little difference between the prepared CNUs (2.94−3.02 eV) (Figure 5b−d). The higher photoexcitation rate of CNUMW, however, has been accompanied by a relatively higher exciton recombination rate, as depicted by its higher photoluminescence (PL) intensity than two of the other CNUs (Figure 5e).

The addition of water to the urea precursor was able to reduce the charge transfer resistance of the resulting C_2N_3, as demonstrated by the smaller arc of the Nyquist plot of CNUH2O compared to CNU (Figure 5f). Nevertheless, microwave treatment of the precursor does not facilitate the charge transfer in the CNUMW but slightly increases its impedance to a higher level than CNU. It was also observed that the transient photocurrent generated by CNUMW was much lower than that of CNU, which can be attributed to the poorer charge transfer that led to less efficient charge separation and rapid recombination of excitons (Figure 5g).

3.3. Photocatalytic Activity. Given the results of characterization, it was evidenced that introducing water to urea would produce a larger yield of C_2N_3 but with inferior surface area and optical and electrochemical properties, which could result in poor photocatalytic performance. Meanwhile, pretreating moisturized urea with microwave energy before calcination has been demonstrated as a promising solution that can be employed to further increase the production yield while attempting to retain the photocatalytic activity of urea-derived C_2N_3.

The photocatalytic activities of CNU, CNUH2O, and CNUMW were evaluated at the optimized conditions of 750 mg L^{-1} of photocatalyst in 25 mg L^{-1} of RB5 solution at pH 7.0 (Figure S3). At the optimum condition, it was observed that CNUMW has the lowest adsorption capacity toward RB5

https://doi.org/10.1021/acsestwater.4c00879
ACS EST Water 2024, 4, 5902−5912

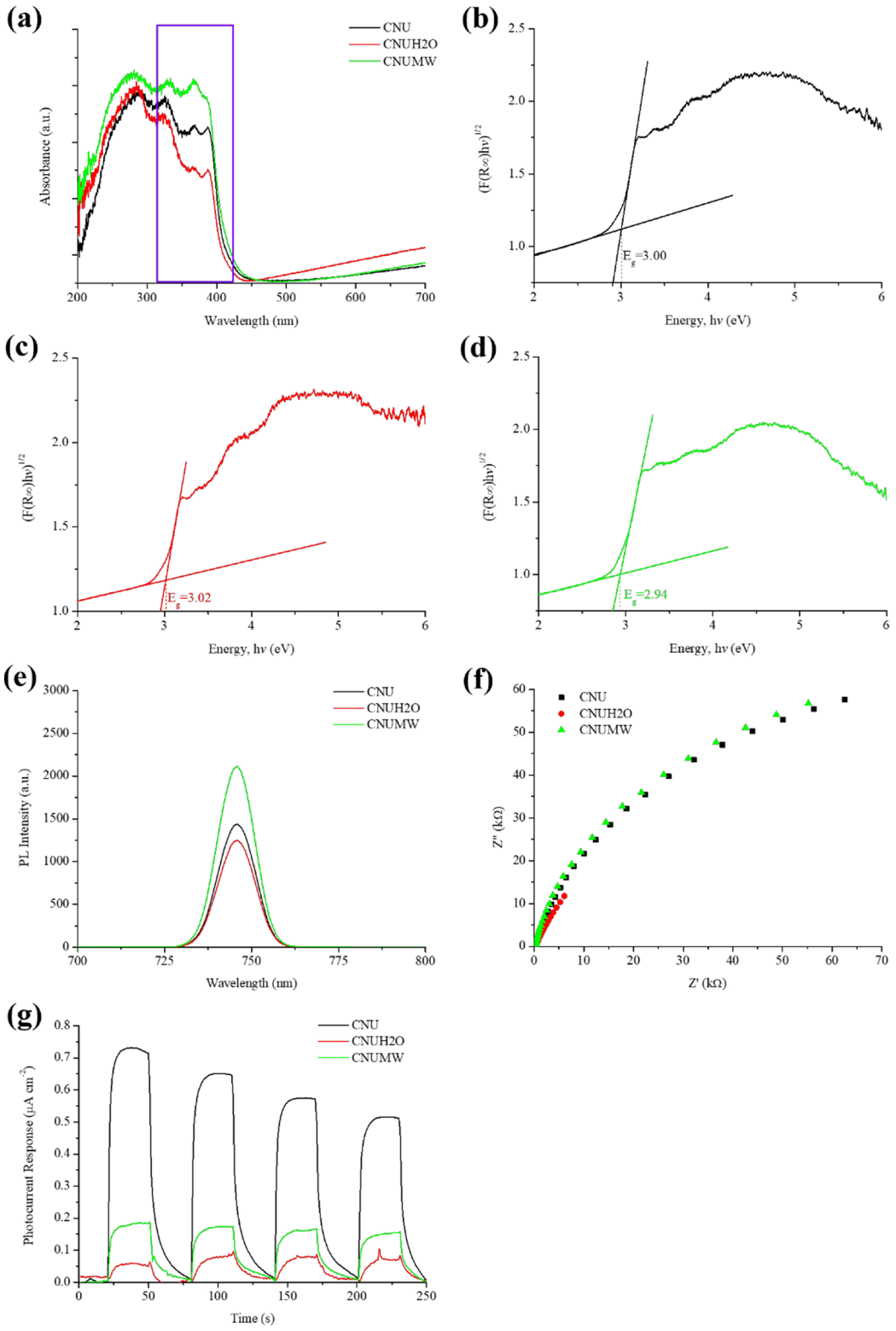

Figure 5. UV−visible spectra (a) and Tauc plots of (b) CNU, (c) CNUH2O, and (d) CNUMW. (e) Overlayered PL spectra of g-C_2N_3. (f) Nyquist plots and (g) transient photocurrent responses of prepared g-C_2N_3.

among the three photocatalysts (Figure 6a). This is because CNUMW contains a higher number of polar oxygen-containing groups on its surface than directly calcined CNU and therefore, has a smaller nonpolar surface area for van der Waals interaction with the nonpolar moiety of RB5.[34] Nevertheless, the rate of RB5 degradation was higher in the presence of CNUMW (0.2160 min^{-1}) than those of CNU (0.0520 min^{-1}) and CNU (0.0942 min^{-1}) (Figure 6b). A highly porous, hydrangea-like morphology could provide CNUMW with a larger contact area for pollutant molecule-catalyst interaction, which effectively increases the frequency of reaction. Despite weaker interaction between the target

https://doi.org/10.1021/acsestwater.4c00879
ACS EST Water 2024, 4, 5902−5912

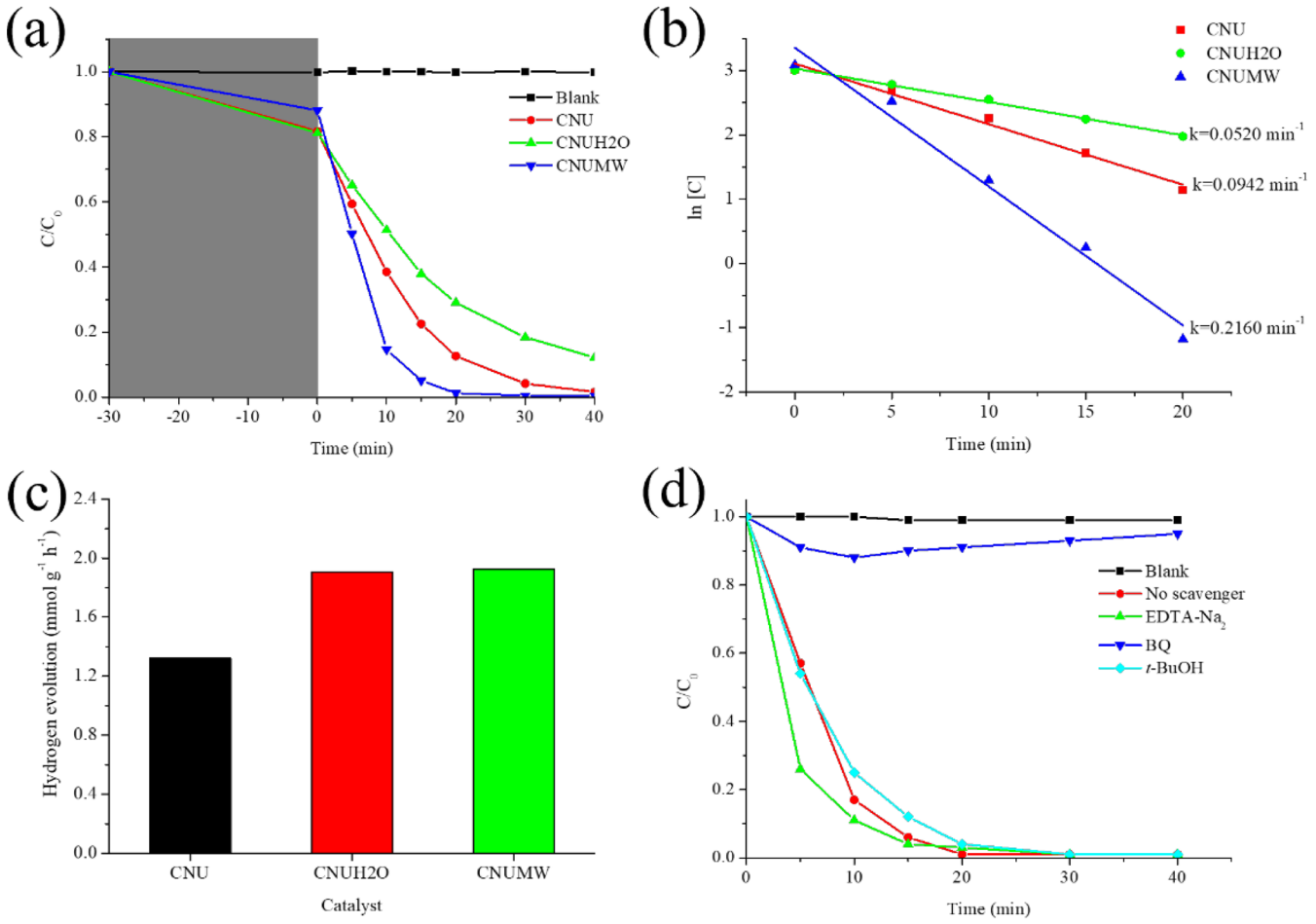

Figure 6. Photocatalytic activity of CNUs in RB5 (a) degradation and (b) kinetic studies. (c) Hydrogen production during photocatalytic degradation of RB5 by as-synthesized CNUs. (d) Scavenging test of CNU-catalyzed RB5 photodegradation (25 mg L^{-1} RB5, 750 mg L^{-1} photocatalyst, pH 7, volume = 25 mL, λ = 420 nm, power = 10 W for dye degradation and 100 W for hydrogen production).

molecules and photocatalyst, a higher visible light absorption capability in the region closer to the band gap energy (Figure 5a,d) could increase the reaction rate. The results show that a larger BET surface area, a smaller band gap, and improved absorption near the Urbach energies region overwhelm the adverse effect of rapid charge recombination and slightly increased impedance, leading to improved photocatalytic activity.

The potential to generate green hydrogen when remediating dye-polluted water was also evaluated by using CNUs. A previous study by Tang et al. showed that g-C_2N_3 is more effective in photocatalytic H_2 evolution than g-C_3N_4 when using sodium sulfide and sodium sulfite as sacrificial agents.[27] They ascribed the superior activity of g-C_2N_3 to its intrinsic spontaneous polarization electric field, which facilitates charge transfer and charge utilization. Our study, under the selected conditions, showed that introducing water into urea produced CNUH2O with a 45% increase in the hydrogen generation rate when compared to that of CNU (Figure 6c). CNUMW with a higher N content in the bulk and a greater O concentration on the surface has a comparable H_2 generation rate to that of CNUH2O (1.93 mmol g^{-1} h^{-1} vs 1.91 mmol g^{-1} h^{-1}, Δ = 1%). The findings of photocatalytic testing demonstrated that in addition to enhanced yield, C_2N_3 synthesized with the assistance of microwave pretreatment successfully retained the high photoremediation efficiency of CNU while boosting its H_2 generation capability.

The reaction mechanism of CNUMW-catalyzed RB5 photodegradation was evaluated by scavenging tests. The result showed that BQ significantly inhibited the rate of photocatalysis, which implied that the dye degradation reaction was propagated via a superoxide radical pathway. This is consistent with the finding that CNUMW has a conduction band potential of −0.52 eV, calculated from the band gap energy (2.94 eV, Figure 6d) and valence band maxima of 2.42 eV (Figure S4), which is lower than the reduction potential of molecular oxygen to the superoxide radical (E = −0.33 eV).[35] It is worth noting that adding EDTA-Na_2 as a hole scavenger slightly improved the rate of RB5 degradation. This is due to the reduced excitons recombination by the hole scavenger and the concurrent formation of reductive radicals (•EDTA) that promoted the photodegradation of RB5.[36]

The performance of the improved hydrangea-like urea-based carbon nitride (g-C_2N_3) photocatalyst was compared to that of other reported metal-free photocatalysts (Table 2). Based on the comparison, it was demonstrated that our catalyst could degrade organic dye at a high rate (>200 × 10^{-3} min^{-1}) comparable to other modified photocatalysts under the irradiation of an energy-efficient, low-power, single-wavelength LED lamp. For photocatalytic H_2 generation, hydrangea-like g-C_2N_3 showed activity significantly higher than that of bulk

https://doi.org/10.1021/acsestwater.4c00879
ACS EST Water 2024, 4, 5902−5912

Table 2. Photocatalysts and Their Activities in Dye Degradation and Hydrogen Generation[a]

Photocatalyst	Dye	Light source, Power	Catalyst loading (mg L^{-1})	Dye concentration (mg L^{-1})	pH	Dye degradation rate ($\times 10^{-3}$ min^{-1})	Sacrificing agent	H_2 evolution rate (mmol g^{-1} h^{-1})	Ref.
Hydrangea-like g-C_2N_3	RB5	LED (λ = 420 nm)							This study
		p =10 W	750	25	7	216	-	-	
		p = 100 W	-	-	7	-	25 mg L^{-1} RB5	1.93	
3D hollow porous aminopyridine rings decorated polymeric carbon nitride	RhB	Xe lamp ($\lambda \geq$ 420 nm) p = 300 W	500	20	-	236	-	-	37
		Metal halide ($\lambda \geq$ 420 nm)p = 500 W	500	-	-	-	10% v/v triethanolamine	2.44	
Bulk carbon nitride	RhB	Xe lamp ($\lambda \geq$ 420 nm) p = 300 W	500	20	-	9.3	-	-	37
		Metal halide ($\lambda \geq$ 420 nm)p = 500 W	500	-	-	-	10% v/v Triethanolamine	0.07	
3D interlinked porous g-C_3N_4	RhB	Xe lamp ($\lambda \geq$ 420 nm) p=300 W	500	20	-	228	-	-	38
		Metal halide ($\lambda \geq$ 420 nm)p = 500 W	500	-	-	-	10% v/v triethanolamine	1.96	
ultrathin crystalline carbon nitride nanosheets	-	Xe lamp ($\lambda \geq$ 420 nm) p = 300 W	333	-	-	-	10% v/v triethanolamine	11.5	39
porous, thin g-C_3N_4 nanosheets	RhB	Xe lamp ($\lambda \geq$ 420 nm) p = 300 W	200	10	-	224	-	-	40
flaky g-C_3N_4	-	Xe lamp ($\lambda \geq$ 420 nm) p = 600 W	250	-	-	-	10% v/v isopropanol	1.28	41
urea/thiourea-based g-C_3N_4	RhB	LED p = 50 W	500	10	-	16.5	-	-	42
fibrous graphitic carbon nitride	-	Sunlight	100	-	-	-	5% v/v methanol	0.08	43
Z-scheme hydrogen-bonded organic frameworks/ g-C_3N_4 nanosheets heterojunction	MO	Xe lamp ($\lambda \geq$ 420 nm) p = 300 W	182	20	-	53.7	-	-	44
			1000	-	-	-	9% v/v triethanolamine	4.45	

[a]RB 5: Reactive Black 5; RhB: Rhodamine B; MB: Methylene Blue; MO: Methyl Orange.

https://doi.org/10.1021/acsestwater.4c00879
ACS EST Water 2024, 4, 5902−5912

carbon nitride, flaky g-C_3N_4, and fibrous graphitic carbon nitride. The photocatalytic activity of organic entity functionalized catalysts was found to be comparable to or slightly higher than that of g-C_2N_3 from this study, possibly due to the use of a higher power light source in experiments. The photocatalytic water splitting activity of Z-scheme hydrogen-bonded organic frameworks/g-C_3N_4 nanosheets heterojunction was 2.3 times higher than hydrangea-like g-C_2N_3, but it has a lower dye degradation rate.

4. CONCLUSION

A microwave-assisted carbon nitride synthesis method has been investigated, and it has been proven effective in increasing the yield by approximately 5 times when compared to conventional preparation. Elemental analysis revealed that the resulting carbon nitride comprised a g-C_2N_3 structure made up of aromatic pentagonal azide and hexagonal triazine. This microwave-treated g-C_2N_3 has a higher surface area than bulk g-C_2N_3 and a greater absorption in the UV-A region close to Urbach energies, which were beneficial in enhancing the photocatalytic activity of g-C_2N_3. The hydrangea-like g-C_2N_3 with twisted hollow tube morphology possesses superior photocatalytic activity as demonstrated by their higher reaction rates of 0.2162 min^{-1} and 1.93 mmol g^{-1} h^{-1} in RB5 degradation and hydrogen generation reactions. It was determined that the dye degradation reaction was mediated by a superoxide radical pathway. This study demonstrated an effective way to produce a unique g-C_2N_3 that is active in both photocatalytic pollutant degradation and energy production.

■ ASSOCIATED CONTENT

Supporting Information

The Supporting Information is available free of charge at https://pubs.acs.org/doi/10.1021/acsestwater.4c00879.

Mott−Schottky plot, IR spectra, photocatalytic RB5 degradation results, and valence band maxima plot of CNUs (PDF)

■ AUTHOR INFORMATION

Corresponding Author

Yang-hsin Shih − *Department of Agricultural Chemistry, National Taiwan University, Taipei 10617, Taiwan;* orcid.org/0000-0002-1326-0720; Email: yhs@ntu.edu.tw

Authors

Kok-Hou Tan − *Department of Agricultural Chemistry, National Taiwan University, Taipei 10617, Taiwan; Cardiff Catalysis Institute, Translational Research Hub, Cardiff University, Cardiff CF24 4HQ, U.K.;* orcid.org/0000-0002-4119-0686

Chen-Yu Lin − *Department of Agricultural Chemistry, National Taiwan University, Taipei 10617, Taiwan*

Complete contact information is available at: https://pubs.acs.org/10.1021/acsestwater.4c00879

Author Contributions

CRediT: **Kok-Hou Tan** conceptualization, data curation, formal analysis, funding acquisition, investigation, methodology, project administration, validation, visualization, writing - original draft; **Chen-yu Lin** investigation; **Yang-hsin Shih** funding acquisition, resources, supervision, writing - review & editing.

Notes

The authors declare no competing financial interest.

■ ACKNOWLEDGMENTS

The authors acknowledge the financial support from the National Science and Technology Council (NSTC) of Taiwan (NSTC 111-2811-E-002-057-MY3 and NSTC 111-WFA-0-110-867). The technical support by Dr. Yao-Chang Lee and Ms. Pei-Yu Huang of the National Synchrotron Radiation Research Centre) TLS Beamline 14A1 was highly appreciated. Authors also thank Ms. C.-Y. Chien of NSTC (National Taiwan University) for the assistance in SEM and TEM experiments. The authors would also like to express gratitude to Professor Stuart H. Taylor for his favor in manuscript proofreading.

■ REFERENCES

(1) Osman, A. I.; Elgarahy, A. M.; Eltaweil, A. S.; Abd El-Monaem, E. M.; El-Aqapa, H. G.; Park, Y.; Hwang, Y.; Ayati, A.; Farghali, M.; Ihara, I.; Al-Muhtaseb, A. H.; Rooney, D. W.; Yap, P. S.; Sillanpää, M. Biofuel Production, Hydrogen Production and Water Remediation by Photocatalysis, Biocatalysis and Electrocatalysis. *Environ. Chem. Lett.* **2023**, *21*, 1315−1379.

(2) Thomas, A.; Fischer, A.; Goettmann, F.; Antonietti, M.; Müller, J.-O.; Schlögl, R.; Carlsson, J. M. Graphitic Carbon Nitride Materials: Variation of Structure and Morphology and Their Use as Metal-Free Catalysts. *J. Mater. Chem.* **2008**, *18* (41), 4893.

(3) Tan, L.; Nie, C.; Ao, Z.; Sun, H.; An, T.; Wang, S. Novel Two-Dimensional Crystalline Carbon Nitrides beyond g-C_3N_4: Structure and Applications. *J. Mater. Chem. A Mater.* **2021**, *9* (1), 17.

(4) Qamar, M. A.; Javed, M.; Shahid, S.; Shariq, M.; Fadhali, M. M.; Ali, S. K.; Khan, M. S. Synthesis and Applications of Graphitic Carbon Nitride (g-C_3N_4) Based Membranes for Wastewater Treatment: A Critical Review. *Heliyon* **2023**, *9* (1), No. e12685.

(5) Raaja Rajeshwari, M.; Kokilavani, S.; Sudheer Khan, S. Recent Developments in Architecturing the G-C_3N_4 Based Nanostructured Photocatalysts: Synthesis, Modifications and Applications in Water Treatment. *Chemosphere* **2022**, *291*, 132735.

(6) Samsudin, M. F.; Bacho, N.; Sufian, S. *Recent Development of Graphitic Carbon Nitride-Based Photocatalyst for Environmental Pollution Remediation*. Intechopen, 2019. DOI: .

(7) Song, X.; Yang, Q.; Yin, M.; Tang, D.; Zhou, L. Highly Efficient Pollutant Removal of Graphitic Carbon Nitride by the Synergistic Effect of Adsorption and Photocatalytic Degradation. *RSC Adv.* **2018**, *8* (13), 7260.

(8) Fidan, T.; Arat, R.; Bayazit, M. K. A Handbook for Graphitic Carbon Nitrides: Revisiting the Thermal Synthesis and Characterization towards Experimental Standardization. *Mater. Res. Express.* **2023**, *10* (9), 095905.

(9) Wang, Z.; Huo, Y.; Fan, Y.; Wu, R.; Wu, H.; Wang, F.; Xu, X. Facile Synthesis of Carbon-Rich g-C_3N_4 by Copolymerization of Urea and Tetracyanoethylene for Photocatalytic Degradation of Orange II. *J. Photochem. Photobiol. A Chem.* **2018**, *358*, 61.

(10) Liu, X.; Xu, X.; Gan, H.; Yu, M.; Huang, Y. The Effect of Different G-C3N4 Precursor Nature on Its Structural Control and Photocatalytic Degradation Activity. *Catalysts* **2023**, *13* (5), 848.

(11) Zhang, W.; Zhang, Q.; Dong, F.; Zhao, Z. The Multiple Effects of Precursors on the Properties of Polymeric Carbon Nitride. *Int. J. Photoenergy* **2013**, *2013*, 685038.

(12) Shi, L.; Liang, L.; Wang, F.; Liu, M.; Chen, K.; Sun, K.; Zhang, N.; Sun, J. Higher Yield Urea-Derived Polymeric Graphitic Carbon Nitride with Mesoporous Structure and Superior Visible-Light-Responsive Activity. *ACS Sustainable Chem. Eng.* **2015**, *3* (12), 3412.

(13) Ye, Z.; Yue, W.; Tayyab, M.; Zhang, J.; Zhang, J. Simple One-Pot, High-Yield Synthesis of 2D Graphitic Carbon Nitride Nano-

sheets for Photocatalytic Hydrogen Production. *Dalton Trans.* **2022**, *51* (48), 18542.
(14) Zhang, L.; Wang, H.; Shen, W.; Qin, Z.; Wang, J.; Fan, W. Controlled Synthesis of Graphitic Carbon Nitride and Its Catalytic Properties in Knoevenagel Condensations. *J. Catal.* **2016**, *344*, 293.
(15) Meng, L.; Ushakova, E. V.; Zhou, Z.; Liu, E.; Li, D.; Zhou, D.; Tan, Z.; Qu, S.; Rogach, A. L. Microwave-Assisted: In Situ Large Scale Synthesis of a Carbon Dots@g-C_3N_4 Composite Phosphor for White Light-Emitting Devices. *Mater. Chem. Front.* **2020**, *4* (2), 517.
(16) Gross, P.; Höppe, H. A. Biuret—A Crucial Reaction Intermediate for Understanding Urea Pyrolysis To Form Carbon Nitrides: Crystal-Structure Elucidation and In Situ Diffractometric, Vibrational and Thermal Characterisation. *Chem.—Eur. J.* **2020**, *26* (63), 14366−14376.
(17) Dong, H.; Guo, X.; Yang, C.; Ouyang, Z. Synthesis of G-C_3N_4 by Different Precursors under Burning Explosion Effect and Its Photocatalytic Degradation for Tylosin. *Appl. Catal., B* **2018**, *230*, 65.
(18) Tischer, S.; Börnhorst, M.; Amsler, J.; Schoch, G.; Deutschmann, O. Thermodynamics and Reaction Mechanism of Urea Decomposition. *Phys. Chem. Chem. Phys.* **2019**, *21* (30), 16785.
(19) Wang, X. L.; Yang, H. G. Facile Fabrication of High-Yield Graphitic Carbon Nitride with a Large Surface Area Using Bifunctional Urea for Enhanced Photocatalytic Performance. *Appl. Catal., B* **2017**, *205*, 624.
(20) Gebreslassie, G.; Bharali, P.; Gebremariam, G.; Sergawie, A.; Alemayehu, E. Graphitic Carbon Nitride with Extraordinary Photocatalytic Activity Under Visible Light Irradiation. In *Lecture Notes of the Institute for Computer Sciences*, 2021; Social-Informatics and Telecommunications Engineering, LNICST, Vol. *385*. .
(21) Yuan, Y. P.; Yin, L. S.; Cao, S. W.; Gu, L. N.; Xu, G. S.; Du, P.; Chai, H.; Liao, Y. S.; Xue, C. Microwave-Assisted Heating Synthesis: A General and Rapid Strategy for Large-Scale Production of Highly Crystalline g-C_3N_4 with Enhanced Photocatalytic H_2 Production. *Green Chem.* **2014**, *16* (11), 4663−4668.
(22) Qiu, P.; Chen, H.; Xu, C.; Zhou, N.; Jiang, F.; Wang, X.; Fu, Y. Fabrication of an Exfoliated Graphitic Carbon Nitride as a Highly Active Visible Light Photocatalyst. *J. Mater. Chem. A Mater.* **2015**, *3* (48), 24237.
(23) Lin, X.; Du, S.; Li, C.; Li, G.; Li, Y.; Chen, F.; Fang, P. Consciously Constructing the Robust NiS/g-C_3N_4 Hybrids for Enhanced Photocatalytic Hydrogen Evolution. *Catal. Lett.* **2020**, *150* (7), 1898.
(24) Praus, P.; Smýkalová, A.; Foniok, K.; Matějka, V.; Kormunda, M.; Smetana, B.; Cvejn, D. The Presence and Effect of Oxygen in Graphitic Carbon Nitride Synthetized in Air and Nitrogen Atmosphere. *Appl. Surf. Sci.* **2020**, *529*, 147086.
(25) Xiong, D.; Zhang, Q.; Verma, S. K.; Bao, X. Q.; Li, H.; Zhao, X. Crystal Structural, Optical Properties and Mott-Schottky Plots of p-Type Ca Doped $CuFeO_2$ Nanoplates. *Mater. Res. Bull.* **2016**, *83*, 141.
(26) Shi, L.-B.; Cao, S.; Zhang, J.; Xiu, X. M.; Dong, H. K. Mechanical Behaviors and Electronic Characteristics on Two-Dimensional C_2N_3 and C_2N_3H: First Principles Calculations. *Physica E Low Dimens. Syst. Nanostruct.* **2018**, *103*, 252−263.
(27) Tang, D.; Shao, C.; Jiang, S.; Sun, C.; Song, S. Graphitic C_2N_3: An Allotrope of g-C_3N_4 Containing Active Azide Pentagons as Metal-Free Photocatalyst for Abundant H_2 Bubble Evolution. *ACS Nano* **2021**, *15* (4), 7208.
(28) Long, X.; Feng, C.; Yang, S.; Ding, D.; Feng, J.; Liu, M.; Chen, Y.; Tan, J.; Peng, X.; Shi, J.; Chen, R. Oxygen Doped Graphitic Carbon Nitride with Regulatable Local Electron Density and Band Structure for Improved Photocatalytic Degradation of Bisphenol A. *Chem. Eng. J.* **2022**, *435*, 134835.
(29) Zhang, Y.; Li, K.; Liao, J.; Wei, X.; Zhang, L. Microwave-Assisted Synthesis of Graphitic Carbon Nitride/CuO Nanocomposites and the Enhancement of Catalytic Activities in the Thermal Decomposition of Ammonium Perchlorate. *Appl. Surf. Sci.* **2020**, *499*, 143875.
(30) You, R.; Dou, H.; Chen, L.; Zheng, S.; Zhang, Y. Graphitic Carbon Nitride with S and O Codoping for Enhanced Visible Light Photocatalytic Performance. *RSC Adv.* **2017**, *7* (26), 15842.
(31) Wan, S.; Xu, J.; Cao, S.; Yu, J. Promoting Intramolecular Charge Transfer of Graphitic Carbon Nitride by Donor−Acceptor Modulation for Visible-light Photocatalytic H_2 Evolution. *Interdiscip. Mater.* **2022**, *1* (2), 294.
(32) Rodríguez, N. A.; Savateev, A.; Grela, M. A.; Dontsova, D. Facile Synthesis of Potassium Poly(Heptazine Imide) (PHIK)/Ti-Based Metal-Organic Framework (MIL-125-NH_2) Composites for Photocatalytic Applications. *ACS Appl. Mater. Interfaces* **2017**, *9* (27), 22941.
(33) Torres-Pinto, A.; Silva, C. G.; Faria, J. L.; Silva, A. M. T. The Effect of Precursor Selection on the Microwave-Assisted Synthesis of Graphitic Carbon Nitride. *Catal. Today* **2023**, *424*, 113868.
(34) Maeda, K.; An, D.; Kuriki, R.; Lu, D.; Ishitani, O. Graphitic Carbon Nitride Prepared from Urea as a Photocatalyst for Visible-Light Carbon Dioxide Reduction with the Aid of a Mononuclear Ruthenium(II) Complex. *Beilstein J. Org. Chem.* **2018**, *14* (Ii), 1806−1812.
(35) Kwon, B. G.; Yoon, J. Superoxide Anion Radical: Principle and Application. *J. Korean Industrial Engineering Chem.* **2009**, *20* (6), 593−602.
(36) Yu, F.; Gong, F.; Yang, Q.; Wang, Y. Fabrication of a Magnetic Retrievable Dual Z-Scheme g-C_3N_4/$BiVO_4$/$CoFe_2O_4$ Composite Photocatalyst with Significantly Enhanced Activity for the Degradation of Rhodamine B and Hydrogen Evolution under Visible Light. *Diam. Relat. Mater.* **2022**, *125*, 109004.
(37) Liu, D.; Zhao, C.; Li, C.; Jia, J.; Chen, M.; Pan, L.; Bai, Y.; Wu, W.; Ni, T. Facile Fabrication of 3D Hollow Porous Aminopyridine Rings Decorated Polymeric Carbon Nitride for Enhanced Photocatalytic Hydrogen Evolution and Dye Elimination. *J. Colloid Interface Sci.* **2023**, *649*, 334−343.
(38) Tian, C.; Li, C.; Zhao, C.; Liu, D.; He, X. A Novel Synthetic 3D Interconnected Porous Carbon-Rich Graphitic Carbon Nitride for Boosting Visible Light Photocatalytic Hydrogen Production and Dye Contaminant Degradation. *Catalysts* **2023**, *13* (10), 1345.
(39) Li, X.; Wu, J.; An, S.; Li, K.; Zhang, J.; Pei, M.; Song, C.; Guo, X. Ultrathin Crystalline Carbon Nitride Nanosheets for Highly Efficient Photocatalytic Pollutant Removal and Hydrogen Production. *ACS Appl. Nano Mater.* **2023**, *6* (13), 11601−11611.
(40) Guo, J.; Sun, Y.; Xiang, R.; Yu, H.; Chen, Z.; Zhang, F.; Liu, F. One-Step Synthesis of Porous Thin-Layered Graphitic Carbon Nitride for Enhanced Photocatalytic Dye Degradation. *Colloids Surf., A* **2023**, *671*, 131600.
(41) Wang, Z.; Wang, J.; Iqbal, W.; Shi, M.; Yang, L.; Chang, N.; Qin, C. Morphology-Effects of Four Different Dimensional Graphitic Carbon Nitrides on Photocatalytic Performance of Dye Degradation, Water Oxidation and Splitting. *J. Phys. Chem. Solids* **2023**, *173*, 111109.
(42) Sewnet, A.; Alemayehu, E.; Abebe, M.; Mani, D.; Thomas, S.; Kalarikkal, N.; Lennartz, B. Single-Step Synthesis of Graphitic Carbon Nitride Nanomaterials by Directly Calcining the Mixture of Urea and Thiourea: Application for Rhodamine B (RhB) Dye Degradation. *Nanomaterials* **2023**, *13* (4), 762.
(43) Karthik, K.; Keerthi; Bernaurdshaw, N. Box−Behnken Design and Experimental Studies on Novel Fibrous g-C_3N_4 towards Water Splitting and Degradation of Indigo Carmine Dye. *Int. J. Hydrogen Energy* **2024**, *57*, 939.
(44) Shi, H.; Feng, D.; Li, H.; Yu, D.; Chen, X. Hydrophilic Hydrogen-Bonded Organic Frameworks/g-C_3N_4 All-Organic Z-Scheme Heterojunction for Efficient Visible-Light Photocatalytic Hydrogen Production and Dye Degradation. *J. Photochem. Photobiol. A Chem.* **2023**, *435*, 114292.

https://doi.org/10.1021/acsestwater.4c00879
ACS EST Water 2024, 4, 5902−5912